Predictive Autonomous Orbit Control Method for Low Earth Orbit Satellites

By Jérôme THOMASSIN,[1)] Maxime ECOCHARD,[2)] and Guillaume Azema[2)]

[1)]*Department of Flight Dynamics, CNES, Toulouse, France*
[2)]*Spaceflight Dynamics Department, Thales Services, Toulouse, France*

The use of Autonomous Orbit Control (AOC) for station-keeping at low altitudes raises the issue of the collision risks management process. The need by ground segment for accurate knowledge of the satellite orbit contrasts with the on-board autonomy and the orbit control reactivity. An intermediate step towards the on-board autonomy of collision alerts is to make AOC more predictable for the ground segment. In this perspective, CNES has studied and developed an algorithmic method enabling AOC to become more predictable by adding a frozen horizon for upcoming maneuvers. This method enables a control of the inclination, right ascension of the ascending node, semi major axis and argument of latitude, and optimizes the orbit eccentricity. At the current stage of planning and development, a frozen horizon of 24h on 850 km altitude orbits leads to reasonable in-track and cross-track error windows of *resp.* ± 3000m and ±1000m. The present algorithm improvement, as the implementation of an additional semi-frozen horizon, enables worthwhile prospects on both the station-keeping and the predictable horizon duration performance, applicable to a wide range of LEO altitudes (typically 450-1000 km).

Key Words: Autonomous Orbit Control, station-keeping, LEO, collision risk

Nomenclature

a	:	semi-major axis
e	:	eccentricity
ω	:	argument of perigee
i	:	inclination
Ω	:	RAAN (Right Ascension of the Ascending Node)
α	:	argument of latitude
ν	:	true anomaly
ΔT	:	long-track difference (TNW frame)
Subscripts		
estim	:	estimated
max	:	maximum
mes	:	predicted at the maneuver date from measurements at current node
targ	:	target
th	:	theoretical

1. Introduction

AOC can provide both significant operations cost reduction and increased mission performance. By controlling the orbit to match a chosen reference, ground operations are significantly reduced and scheduling becomes highly predictable. AOC gains in value for very low Earth orbit satellites, when the effects of atmospheric drag must very often be compensated for. Historically, AOC has been successfully experimented on Demeter, a Myriade satellite (CNES line of micro-satellites), with an in-plane control[1)].

Even if the use of AOC enables easing the station-keeping management, the assessment of the debris collision risk becomes more complicated. Indeed, station-keeping at low altitude involves frequent orbit control maneuvers. Moreover, the increasing number of monitored objects in LEO leads to heighten the collision alerts during station-keeping operational phase.

The collision alerts management process requires from ground segment an accurate knowledge of the satellite orbit, within 8 hours at least and classically within 12 to 24 hours to enable the risk determination and the implementation of an avoidance strategy. The current AOC use does not enable this fine knowledge because the maneuvers scheduling and completion are not-predictive - the future maneuvers are known on-board just before their occurrences. A method developed by CNES is to perform ground simulations of all future possible satellite trajectories[2)]. This method requires several daily dialogs between ground services and the implementation of calculation loops.

This issue has led CNES to study and develop another algorithmic method for both in-track and cross-track controls. This method enables AOC to become more predictable by adding a frozen horizon for upcoming maneuvers. In other words, the predictive AOC method particularly enables the ground segment team to be warned soon enough of the future maneuvers computed by the AOC. If the future maneuvers are known, the orbit is fully predictable and the position of the spacecraft within this period is known in advance within a better accuracy. This is particularly useful to assess the debris collision risk because the predicted satellite trajectory can be compared to known near debris ephemeris.

2. Background information

The maneuver computation of AOC system is performed at each ascending node crossing, based on the determination of needed correction on orbital parameters, in order to keep the

ground tracks in a specified window.
The AOC algorithms and settings have been implemented in order to obtain a generic tool for different satellites, missions and orbits. For this reason the control is based on the orbital mechanics rather than on the use of a classic controller (e.g. PID controllers…).

2.1. Orbits

The reference orbit is a "2D" simplified analytic model (depending on both the argument of latitude and the longitude of the ascending node) used by the mission for long-term planning. The station-keeping performances are those given by the in-track and cross-track deviations from this reference orbit. The expected results in terms of performance depends on on-ground antennas stations requirements (tracking and telemetry budget link).

The guidance orbit used by AOC for its control is an analytical 1D guideline at the ascending node, consistent with the reference orbit.

Reference and guidance orbits take into account the Earth potential effects. The orbits as part of this study are low-altitudes orbits for Earth observation missions. They are near-polar, sun-synchronous, with frozen eccentricity and with repeating ground tracks. The altitude range is from 450 to 1000 km.

2.2. Constraints

AOC is limited on its maneuver placements. It cannot perform all kind of maneuvers on every argument of latitude, depending on system constraints (e.g. solar glare on optical instrument), and mission constraints.

It is assumed that mission could not be conducted as same time as orbital control and has priority over it. That means the provided time slots for station keeping maneuvers correspond to periods useless for the mission. Therefore, the orbit control method has to be robust to a busy mission scheduling, involving narrow maneuver opportunities, on restrained orbit positions.

2.3. Orbit control

The main orbital perturbations taken into account for the orbital control include the effects of solar and lunar gravitation, solar radiation pressure, terrestrial tides and atmospheric drag. Again, note that geopotential effects are included inside reference and guidance orbit models.

Two independent controllers manage the in-plane and out-of-plane station-keeping, leading to two kinds of maneuvers.

The in-plane controller regulates both the semi major axis and the argument of latitude and optimizes the impact on eccentricity. This controller commands a semi major axis increment that is converted to a velocity increment. Maneuvers will be performed with a single thrust due to the difficulty of ensuring maneuvers slots with opposite arguments of latitude.

The out-of-plane controller regulates both the inclination and the right ascension of the ascending node. This controller commands an inclination increment that is converted to a velocity increment. It is built upon developed principles on previous works[3].

Eq. (1) shows the set of orbital parameters used to describe the satellite motion.

$$\begin{pmatrix} a \\ ex = e * cos(\omega) \\ ey = e * \sin(\omega) \\ i \\ \Omega \\ \alpha = \omega + \nu \end{pmatrix} \quad (1)$$

3. Operating principle of the predictive AOC

When the satellite crosses the ascending node, the following steps (Fig. 1) come one after the other:

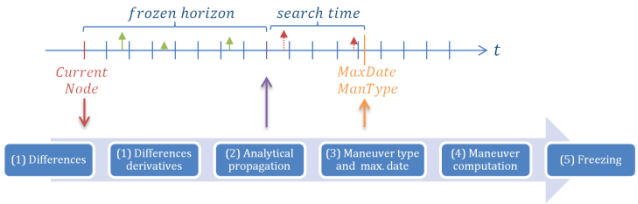

Fig. 1. Operating principle of the predictive AOC.

3.1. Current state

The first step is to compute the differences $(\Delta ex, \Delta ey, \Delta\Omega, \Delta\alpha)$ between the guidance parameters and the measured orbit. From these differences and previous differences (stored on-board), the derivatives of the differences are computed using polynomial curve fitting. Indeed, these computations are based on basic behavioral assumptions: linear or quadratic trend of the orbital parameters differences within the frozen horizon. The orbital state is defined by the orbital parameters differences and their derivatives.

3.2. Propagated state after the frozen horizon

From the current node state, the key step of the predictive AOC is to perform an on-board analytical propagation in order to determine a future theoretical state after the frozen horizon. This propagator is based on the same behavioral assumptions as for the derivatives computations. Moreover, this theoretical future state takes into account the impact of the execution of maneuvers positioned on the frozen horizon (green arrows in Fig. 1).

3.3. Search time determination

The third step is the determination of the next maneuver type and latest date.

From the propagated state, another analytical propagation (using again the same assumptions) is performed to determine the different horizons before crossing a threshold of the control box. The first predicted crossing ($\Delta\alpha$ *or* $\Delta\Omega$) determines the manoeuver type (semi-major axis or inclination). The corresponding date determines the maximal maneuver realization date. Thus, a research zone is marked out (between the end of the frozen horizon and this date) in which the optimal maneuver will be computed.

3.4. Optimal maneuver computation

Depending on the maneuver type defined in the previous step, the semi-major axis search maneuver algorithm or the inclination search maneuver algorithm is used for the optimal maneuver determination, among the available maneuver slots.

If the maneuver to be computed is an inclination maneuver, the list of the inclination slots (within the search period) is browsed through in reverse chronological order. As soon as a slot including a node is found (ascending or descending), an analytical propagation from the state after the frozen horizon to the maneuver realization date (at the node) is performed. Finally, the velocity command is computed to determine the velocity increment.

If the maneuver to be computed is a semi-major axis maneuver, an optimal maneuver selection criterion is first determined according to the current eccentricity: maximization of the corrected eccentricity quantity or maximization of the velocity increment. Then, the list of the semi-major axis slots (within the search period) is browsed through. For each slot, the maneuver computation is executed. Each achievable maneuver is graded according to the selection criterion. At the end, the maneuver with the highest grade is chosen.

Once the date and the velocity increment have been computed, the maneuver is validated, modified or cancelled depending on the propulsion system limitations.

3.5. Freezing

The last step is the frozen horizon updating.

Once the optimal maneuver is determined, two cases can occur (red dotted arrows in Fig. 1): either the maneuver is located in the first orbit following the current frozen horizon, either not. In the first case, the maneuver is frozen (date and velocity increment). Otherwise, the computed maneuver is discarded and the process will be repeated at the next ascending node.

4. Inclination maneuvers

4.1. Command strategy

The inclination controller is based on the natural trend of both the inclination and the RAAN. For our tested cases, the inclination difference naturally increases (top left graph in Fig. 2) at the same time as the RAAN differences evolves parabolically (top right graph in Fig. 2). It is necessary to maneuver just before a threshold ($\Delta\Omega_{max}$) is crossed.

From the orbital state at the maneuver date ($\Delta\Omega_{mes}$, $\Delta\dot{\Omega}_{mes}$), the command $\Delta\dot{\Omega}_{COM\ INC}$ targeting a theoretical parabola ($\Delta\Omega_{targ}$, $\Delta\dot{\Omega}_{targ}$) tangential to the lower threshold ($-\Delta\Omega_{max}$) have to be computed (bottom graph in Fig. 2).

In the nominal case, the orbital state at the maneuver date is $\Delta\dot{\Omega}_{mes} > 0$ (drift to the right) and $\Delta\Omega_{mes} > -\Delta\Omega_{max}$ (targeting the theoretical parabola is possible). In this case, the command (simply based on quadratic equations) is:

$$\Delta\dot{\Omega}_{COM\_INC} = -\sqrt{2\Delta\ddot{\Omega}_{th}}\sqrt{\Delta\Omega_{max} + \Delta\Omega_{mes}} - \Delta\dot{\Omega}_{mes} \quad (2)$$

Where

$$\Delta\ddot{\Omega}_{th} = -\dot{\Omega}\tan(i)\frac{di}{dt}_{th} \text{ with } \frac{di}{dt}_{th} = f(perturbations) \quad (3)$$

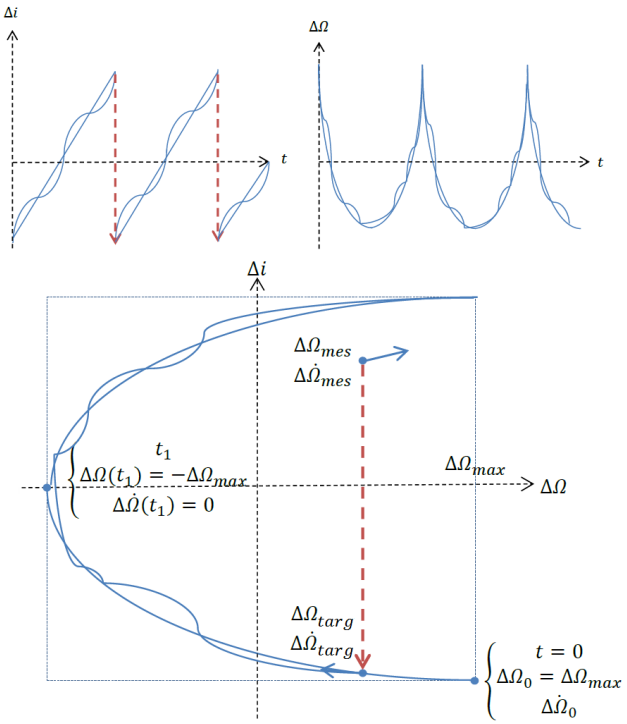

Fig. 2. Inclination maneuvers strategy.

If the drift is to the left, outside the target parabola ($\Delta\dot{\Omega}_{mes} < 0$ and $\Delta\Omega_{mes} < -\Delta\Omega_{max}$), a command targeting no drift is computed:

$$\Delta\dot{\Omega}_{COM\_INC} = -\Delta\dot{\Omega}_{mes} \quad (4)$$

This command prevents from crossing even more the lower threshold but obviously produced an overconsumption.

4.2. Inclination secular effects

The inclination drift is mainly caused by three sources of perturbation: the Sun and Moon gravity potentials, the atmospheric drag and the terrestrial tides.

The *di/dt* caused by a third-body (secular and long-period effects) is computed using the following equation[4]:

$$\frac{di}{dt} = \frac{3}{2}\frac{\mu}{n\,d^3}\frac{Z}{\sqrt{1-e^2}}\left(\cos\omega\,(1+4e^2)\,X - \sin\omega\,(1-e^2)\,Y\right) \quad (5)$$

Where:

- X,Y,Z: components of the unit vector directed from the centre of the Earth to the 3rd body in the (P,Q,W) perifocal coordinate system;
- d: distance between the centre of the Earth and the 3rd body;
- μ: gravitational constant of the 3rd body;
- n: orbit mean motion

The effects of both the atmospheric drag and the terrestrial tides are taken into account measuring the past total drift and removing the known third-body drift. The averaged resulting drift is considered constant for the next $\Delta\Omega$ half-parabola.

4.3. Velocity increment

Once the command is computed, standards flight dynamics equations[5] are used to convert the command into orbital increment (Eq. (6)) and then into velocity increment (Eq. (7)).

$$\Delta\imath = \Delta\dot{\Omega}_{COM\_INC}/k_{\Omega\_i} \quad (6)$$

$$\Delta v = \Delta i * v \quad (7)$$

5. Semi-major axis maneuvers

5.1. Command strategy

The semi-major axis controller is based on the natural trend of both the semi-major axis and the argument of latitude. Naturally, the semi-major axis difference decreases (top left graph in Fig. 3) at the same time as the argument of latitude difference evolves parabolically (top right graph in Fig. 3). It is necessary to maneuver just before a threshold ($\Delta\alpha_{max}$) is crossed.

From the orbital state at the maneuver date ($\Delta\alpha_{mes}$, $\Delta\dot{\alpha}_{mes}$), the command $\Delta\dot{\alpha}_{COM\_SMA\_UP}$ targeting a theoretical parabola ($\Delta\alpha_{targ}$, $\Delta\dot{\alpha}_{targ}$) tangential to the lower threshold ($-\Delta\alpha_{max}$) have to be computed (bottom graph in Fig. 3).

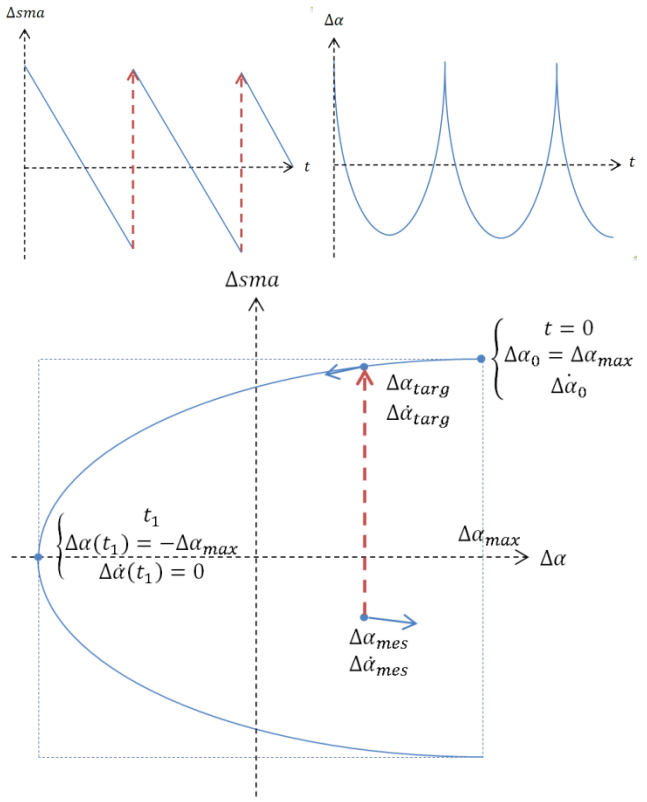

Fig. 3. Semi-major axis maneuvers strategy.

In the nominal case, the orbital state at the maneuver date is $\Delta\dot{\alpha}_{mes} > 0$ (drift to the right) and $\Delta\alpha_{mes} > -\Delta\alpha_{max}$ (targeting the theoretical parabola is possible). In this case, the command (simply based on quadratic equations) is:

$$\Delta\dot{\alpha}_{COM\_SMA\_UP} = -\sqrt{2\Delta\ddot{\alpha}_{estim}}\sqrt{\Delta\alpha_{max} + \Delta\alpha_{mes}} - \Delta\dot{\alpha}_{mes} \quad (8)$$

Where

$$\Delta\ddot{\alpha}_{estim} = f(perturbations) \quad (9)$$

If the drift is to the left ($\Delta\alpha_{mes} < 0$), a command targeting no drift is computed:

$$\Delta\dot{\alpha}_{COM\_SMA\_DOWN} = -\Delta\dot{\alpha}_{mes} \quad (10)$$

This command prevents from crossing the lower threshold but obviously produced an overconsumption.

The control box thresholds are adjusted depending on the predicted eccentricity differences (for each argument of latitude) and the predicted RAAN differences using Eq. (11).

$$\frac{\Delta T}{a} = 2(\Delta ex * sin(\alpha) - \Delta ey * cos(\alpha)) + \Delta\Omega * cos(i) + \Delta\alpha \quad (11)$$

5.2. Velocity increment

Once the command is computed, standard flight dynamics equations[5] are used to convert the command into orbital increment (Eq. (12)) and then into velocity increment (Eq. (13)).

$$\Delta a = \Delta\dot{\alpha}_{COM\_SMA}/k_{\alpha\_a} - k_{\alpha\_i}\,\Delta i\,/\,k_{\alpha\_a} \quad (12)$$

$$\Delta v = \frac{\Delta a}{2a} * v \quad (13)$$

6. Simulation results and predictive AOC performance

A validation simulation campaign has been achieved under specific conditions in order to cross-check the results with expected behaviors. The campaign has shown that the predictive autonomous orbit control algorithms are successful at keeping the satellite within the control box. After this validation, the inclination controller and the semi-major axis controller have been studied independently of each other. It should be noted that the aim of this simulation campaign is to validate the principles of this orbital control method. At this step of development, the control configuration is not yet maximized.

6.1. Inclination controller

The simulations have been conducted in this configuration: low orbit (450km altitude), strong solar activity, out-of plane maximum relative position: +/- 1000m.

The first remark concerning the inclination controller is that the controller isn't constraining in terms of frozen horizon in comparison with the semi-major axis controller. Indeed, the dynamics is slower (i.e. a maneuver is rarely required below 100 days) and the orbital perturbations at stake are more predictable (i.e. the forces modelling are better).

In terms of figures, 3 to 4 maneuvers are required per year and the total velocity increment is about 2 m/s. These results are consistent with standard CNES satellites on similar orbits.

6.2. Semi-major axis controller

The simulations have been conducted in the worst-case configuration: low orbit (450km altitude), strong solar activity, in-track maximum relative position: +/- 3000m. In this use-case, the strong solar activity causes a daily decrease of the semi-major axis that can exceed 150m per day.

The simulation campaigns have shown that the transition phase between a perfect control (no control box crossings) and a sudden degraded one is located in a frozen horizon from 6 to 9 orbits (cf. blue bottom curve in Fig. 4). In other words, the predictability duration is between 9h30 to 14h. This duration is compliant with an emergency implementation of avoidance maneuver by the ground, but requires to be extended to 18 hours at least, even to 24 hours rather, to ease daily operations.

In terms of figures, about 700 maneuvers are required per year (about 1.9 per day) and the yearly velocity increment is about 33 m/s (around 0.05 m/s per maneuver).

6.3. Limitation of the predictive AOC

The semi-major axis lowering, and the parabolic behavior of the relative argument of latitude as well, are caused by the atmospheric drag effects. These effects depend on the air density, which depends on the solar activity. But, the solar flux is (currently) unpredictable within the regarded horizon. The following assumption from the analytical propagator is therefore limited: the argument of latitude acceleration (and by extension the solar flux) is constant from the current node to the end of the frozen horizon.

The argument of latitude acceleration prediction error is the main problem of the semi-major axis controller. It increases according to the frozen horizon (cf. blue top curve in Fig. 4) and leads to more in-track crossings causing a drop in performance (cf. blue bottom curve in Fig. 4). In a perfect world, where the solar activity would be near constant, the acceleration prediction error would be almost zero (cf. red top curve in Fig. 4). In this case, the predictive AOC would be able to reach a much longer frozen time (cf. red bottom curve in Fig. 4).

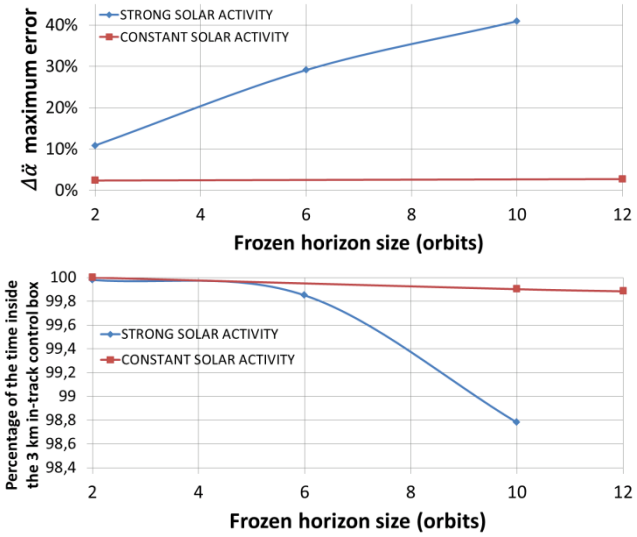

Fig. 4. Predictive AOC performance and limitation for a 450km-altitude orbit.

7. Prospects

The orbit control method described in this paper is still under development and could lead to a better control configuration. In the same way, algorithm improvements could lead to a better trade-off between station-keeping performance and predictability horizon.

First results are promising despite deliberate strong mission constraints for all tested cases, impacting the station-keeping achievement. Above 800km altitude, orbits are fully predictable with this method.

Predictability horizon decreases for lower altitude orbits in strong solar activity period due to the increase of atmospheric drag. The achievable predictability decline is caused by the variability of the solar activity and the difficulty to predict the evolution of this perturbation in this horizon.

The solution presently under development is to add a second maneuvers horizon on which in-plane maneuvers are adjustable in amplitude but with a frozen date of achievement. This maneuver flexibility enables to reach a 24 hours predictability horizon, while enabling more reactivity to atmospheric drag variations.

For risk determination, ground segment has to quantify all the trajectory uncertainties. These uncertainties include classical uncertainties as maneuver achievement errors and navigation errors, and also uncertainties due to the addition of this maneuver flexibility range. Freezing the maneuver dates in this semi-frozen horizon is useful for avoiding discrete events as maneuver jumps, thus preserving a Gaussian error propagation law.

The tuning of the maneuver flexibility range is a trade-off between expected variability for ensuring station-keeping and the limitation of maneuver uncertainties for a reliable collision risk estimate.

A description of overall predictability horizon composed of frozen and semi-frozen horizons is provided in Figure 5.

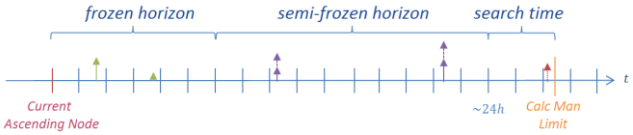

Fig. 5. Overall predictability horizon.

The implementation of the semi-frozen horizon helps to counter the strong variability of the acceleration of the argument of latitude. Parallel studies have been carried out to find an appropriate modeling of the prediction of this parameter, based on past measurements or integrating external data. Results are not yet tangible for this way of improvement. Another option is the use of neural network for the atmospheric density forecast on short-term periods. This solution has been studied by the University of Florida[6]. Nevertheless, this method is slow and complex and needs to be in compliance with on-board processing in terms of computing time, performance and activation frequency.

In contrast with the argument of latitude control, the inclination control is highly efficient for the whole range of altitude.

Further improvements will consist of the addition of a self-tuning threshold and the addition of a terrestrial tides model. They could lead to decrease the number of maneuvers for out-of-plane control.

8. Conclusion

The Predictive Autonomous Orbit Control method is a first step towards an on-board automation of the collision risk management.

This method provides an efficient autonomous station-keeping while enabling an accurate knowledge of the trajectory in a time horizon long enough to manage the collision risk identification and avoidance, by ground segment. In a second development stage, the collision management is expected to be performed by the satellite itself.

Acknowledgments

Authors would like to address thanks to all those people who provided technical support during the realization of this first step of R&D study.

References

1) Lamy, A., Charmeau, M.C, Laurichesse, D., Grondin, M. and Bertrand, R.: Experiment of Autonomous Orbit Control on Demeter, ISSFD2004, Munich, Germany.
2) Bataille, N., Azema, G.: Collision Risk Management for Autonomous Spacecraft, IAC2016, Guadalajara, Mexico.
3) Julien, E. and Lamy, A.: Out-of-plane Autonomous Orbit Control, ISSFD2011, São José dos Campos, Brazil.
4) Lamy, A. and Azema, G.: Selection and optimization of a constellation of satellites for continuous zonal coverage, ISSFD2009, Toulouse, France.
5) CNES, Mécanique Spatiale – Tome I, 1995, p. 794 to 796.
6) Pérez, D.: A Technical Notes – Differential Drag-Based Reference Trajectories for Spacecraft Relative Maneuvering Using Density Forecast, University of Florida, 2016.